Model for the Particle Size, Overpotential, and Strain Dependence of Phase Transition Pathways in Storage Electrodes: Application to Nanoscale Olivines

M. Tang, H.-Y. Huang, N. Meethong, Y.-H. Kao, W. C. Carter, and Y.-M. Chiang

Department of Materials Science and Engineering, Massachusetts Institute of Technology, Cambridge, Massachusetts 02139

Received November 21, 2008. Revised Manuscript Received February 15, 2009

In the drive toward improved electrical energy storage for applications ranging from wireless devices to electric vehicles to grid stabilization, nanoscale materials are of growing interest as ion storage electrodes. Nanoscale olivines based on LiMPO$_4$ (M = Fe, Mn, Co, Ni) are one class of compounds for which recent experimental developments reveal very different phase transition and solid-solubility behavior compared to larger particles. The olivines may be an exemplar for generalized behavior for which metastable crystalline or amorphous phases are produced under the large driving forces incurred during electrochemical reactions. Here we use a diffuse-interface thermodynamic model to assess the conditions under which amorphous phase transitions may occur in nanoscale LiMPO$_4$ particles. There are three central conclusions. First, assuming as with similar solids that the amorphous phase has the lower surface energy, it is found that an initially crystalline phase may undergo amorphization during cycling when the particle size is below a critical value. Second, the effect of applied electrical overpotentials on the phase stability is evaluated for the first time, and is found to strongly influence the phase transition pathways of small particles. Third, the tendency to amorphize is significantly affected by the magnitude of the misfit strain between the lithiated and delithiated crystalline phases. It is shown that there exists a critical misfit strain above which the preferred transformation pathway is amorphization, regardless of the particle size. We use these results to interpret experimentally observed behavior of olivines, including data that up to now have been unexplained.

1. Introduction

Olivine lithium metal phosphates have emerged as important cathode materials in high power batteries for a wide range of applications from power tools to electric vehicles to grid-level power quality.[1−3] It has been shown that particle size reduction and aliovalent doping of pure olivines such as LiFePO$_4$ results in significant changes in phase transition behavior,[4−9] which have a profound impact on battery performance. Recent experiments by Meethong et al.[6] revealed a pronounced size-dependence of the miscibility gap between the endmember olivines FePO$_4$ and LiFePO$_4$ and suggested that a complete solid solution would occur below a critical particle size.[9] In addition, nanosized olivine LiFePO$_4$ and LiMnPO$_4$ particles have been shown to form noncrystalline phases upon cycling.[7] Even at large particle sizes, amorphous interfacial zones have been reported in chemically delithiated LiFePO$_4$.[10]

The appearance of disordered structures in nanoscale olivine particles could result from the influence of surface thermodynamics and an increased surface-to-volume ratio. Disordered (amorphous or liquid) structures generally have lower surface energies than their crystalline counterparts. This is the underlying reason for surfaces in metals and in ice to form a liquidlike film below the bulk melting point, a phenomenon known as surface premelting.[11−13] Similar phenomena occur in multicomponent oxides, where nanometer-thick features referred to as surficial amorphous films (SAFs)[14−17] have been found to form in several systems under conditions where the amorphous/liquid phase is only metastable. Such surficial films are not simply thin layers of a bulk phase, but have unique interfacial structures and

* Corresponding author. E-mail: ychiang@mit.edu.

(1) Macilwain, C. *Nature* **2006**, *444*, 17.
(2) Chu, A. Development of HEV Batteries with Lithium Iron Phosphate Cathodes. *Proceedings of the Sixth International Advanced Automotive Battery Conference*; Baltimore, MD, May 15−19, 2006; Advanced Automotive Batteries: Oregon House, CA, 2006.
(3) http://www.A123Systems.com.
(4) Chung, S.-Y.; Bloking, J. T.; Chiang, Y.-M. *Nat. Mater.* **2002**, *1*, 81.
(5) Meethong, N.; Huang, H.-Y.; Speakman, S. A.; Carter, W. C.; Chiang, Y.-M. *Adv. Funct. Mater.* **2007**, *17*, 1115.
(6) Meethong, N.; Huang, H.-Y.; Carter, W. C.; Chiang, Y.-M. *Electrochem. Solid-State Lett.* **2007**, *10*, A134.
(7) Meethong, N.; Kao, Y.-H.; Tang, M.; Huang, H.-Y.; Carter, W. C.; Chiang, Y.-M. *Chem. Mater.* **2008**, *20*, 6189.
(8) Delmas, C.; Maccario, M.; Croguennec, L.; Le Cras, F.; Weill, F. *Nat. Mater.* **2008**, *7*, 665.
(9) Gibot, P.; Casas-Cabanas, M.; Laffont, L.; Levasseur, S.; Carlach, P.; Hamelet, S.; Tarascon, J. M.; Masquelier, C. *Nat. Mater.* **2008**, *7*, 741.
(10) Chen, G. Y.; Song, X. Y.; Richardson, T. J. *Electrochem. Solid State Lett.* **2004**, *9*, A295.
(11) Frenken, J. W. M.; Maree, P. M. J.; van der Veen, J. F. *Phys. Rev. B* **1986**, *34*, 7506.
(12) Dash, J. G.; Fu, H.; Wettlaufer, J. S. *Rep. Prog. Phys.* **1995**, *58*, 115.
(13) Dash, J. G.; Rempel, A. M.; Wettlaufer, J. S. *Rev. Mod. Phys.* **2006**, *78*, 695.
(14) Luo, J.; Chiang, Y.-M. *Acta Mater.* **2000**, *48*, 4501.
(15) Luo, J.; Chiang, Y.-M.; Cannon, R. M. *Langmuir* **2005**, *21*, 7358.
(16) Luo, J. *Crit. Rev. Solid State Mater. Sci.* **2007**, *32*, 67.
(17) Luo, J.; Chiang, Y.-M. *Annu. Rev. Mater. Res.* **2008**, *38*, 227.

10.1021/cm803172s CCC: $40.75
Published on Web 03/19/2009

compositions with thermodynamic stability. For example, the disordered layers in an SAF have an equilibrium thickness, as well as compositions that are generally distinct from those of any bulk phases found under the same conditions.

The total free energy of a particle includes volumetric and surface contributions. When particle size decreases, the surface energy accounts for an increasingly larger fraction of the total particle energy. A disordered phase that is only metastable as a bulk phase may become thermodynamically stable at sufficiently small particle sizes if the disordered state has lower surface energy. Such phase conversion behavior has been demonstrated in other material systems. For example, using high-temperature oxide melt solution calorimetric measurements,[18] amorphous zirconia (ZrO_2) was found to be stabilized in nanometer particles at room temperature in preference to the crystalline monoclinic phase. A related size-dependent phenomenon is the suppression of melting point in nanocrystalline metal particles.[19] Compared to zirconia, size-dependent phase stability may be even more pronounced in MPO_4 compounds (where M is a 3+ cation) that have crystalline phases isostructural with SiO_2. For instance, the stable high temperature phase of $FePO_4$ may be viewed as a "III−V" structural analog to quartz SiO_2. Such compounds are often good glass formers, suggesting that there is a relatively small difference between the volumetric free energies of their crystalline and amorphous phases, as is the case in SiO_2. Hence a relatively large crossover particle size for amorphous phase stability in these metal phosphates might be expected.

In addition to particle size effects, the applied electrical potential is a fundamental parameter that may alter phase stability in the case of electrically driven phase transformations. Despite the widespread occurrence of cycling-induced phase transitions in solid-state electrochemistry, to the best of our knowledge, the influence of the overpotential on phase stability has not been explicitly treated. From the model developed herein, we illustrate the important and potentially dominant role of the overpotential. (It is recognized that there are many specific overpotentials that arise in electrochemical systems. We will use the term "overpotential" to describe the difference between the electrical potential imposed on a particle, and the equilibrium electrical potential corresponding to the composition and phase state of the particle.) Such phenomena may have great practical importance considering the widely varying overpotentials incurred during use of electrochemical devices such as rechargeable batteries and fuel cells.

Here we use a diffuse-interface model to first determine the energetically stable state of particles with respect to their near-surface structure and composition. The energetics and kinetics of possible phase transition pathways during delithiation of model olivines $LiMPO_4$ are then considered. The energy barriers of competing transformation routes, i.e., a direct crystalline-to-crystalline transformation (the conventional picture) versus a set of crystalline-to-amorphous phase pathways, are evaluated as a function of (1) particle size, (2) applied overpotential, and (3) misfit strain. Each of these parameters is shown to be critically important in determining the conditions under which an amorphous phase will participate in the phase transformation process. We use the results to explain several observations in the literature that to this point have not been satisfactorily explained.

2. Diffuse-Interface Model

As previously discussed,[5] the minimization of elastic energy, surface energy anisotropy, and Li diffusion anisotropy together determine the phase transformation morphology of a crystalline particle, which in general is anisotropic. Thus the so-called "core−shell" model[25] does not apply in most cases.[5,26] Nonetheless, in the present work, we adopt a spherical particle geometry and assume isotropic physical properties for simplicity in the mathematical treatment, and to make the resulting physical phenomena as transparent as possible. (In future refinements, crystalline anisotropy may of course be introduced. All else being equal, crystalline surfaces of higher energy are expected to preferentially amorphize. Anisotropic surface amorphous films have been observed in other systems.[14−17]) The free energy state of a single particle is characterized by its lithium concentration, the state of structural order, and the elastic deformation within the particle. The lithium concentration, c, corresponds to the molar fraction of occupied Li sites in Li_cFePO_4 with $c = 1$ and 0 representing stoichiometric olivine $LiFePO_4$ (triphylite) and $FePO_4$ (heterosite), respectively. The second variable η, often referred to as crystallinity, characterizes the deviation of the local structure from the perfect crystalline state: $\eta = 1$ denotes a crystalline structure, while $\eta = 0$ represents a completely disordered state. A partially ordered structure thus has an η value between 0 and 1. As described in previous literature,[20,21] the crystallinity variable can be related to underlying atomistic structures by proper coarse-graining schemes. In general the values of c and η are nonuniform within the particle, but as in all diffuse-interface models, both variables are assumed to vary smoothly and continuously in space. Similar diffuse-interface (or phase-field) models have previously been applied to the study of solid−liquid interfaces and grain boundary structures.[22−24] In the present case, any inhomogeneous distribution of c and η also results in a spatial variation of the lattice parameter within the particle, thereby giving rise to elastic deformation. Experimental data[5,7,10] suggest that the interface between olivine $LiFePO_4$ and $FePO_4$ may be coherent, semicoherent, or completely incoherent. The dependence of the miscibility gap on crystallite size and composition[5−7] causes the coexist-

(18) Pitcher, M. W.; Ushakov, S. V.; Navrotsky, A.; Woodfield, B. F.; Li, G.; Boerio-Goates, J.; Tissue, B. M. *J. Am. Ceram. Soc.* **2005**, *88*, 160.
(19) Buffat, Ph.; Borel, J.-P. *Phys. Rev. A* **1976**, *13*, 2287.
(20) Bishop, C. M.; Carter, W. C. *Comput. Mater. Sci.* **2002**, *25*, 378.
(21) Tang, M.; Carter, W. C.; Cannon, R. M. *Phys. Rev. B* **2006**, *73*, 024102.
(22) Warren, J. A.; Kobayashi, R.; Lobkovsky, A.; Carter, W. C. *Acta Mater.* **2003**, *51*, 6035.
(23) Granasy, L.; Pusztai, T.; Borzsonyi, T.; Warren, J. A.; Douglas, J. F. *Nat. Mater.* **2004**, *3*, 645.
(24) Tang, M.; Carter, W. C.; Cannon, R. M. *Phys. Rev. Lett.* **2006**, *97*, 075502.
(25) Srinivasan, V.; Newman, J. *J. Electrochem. Soc.* **2004**, *151*, A1517.
(26) Laffont, L.; Delacourt, C.; Gibot, P.; Wu, M. Y.; Kooyman, P.; Masquelier, C.; Tarascon, J. M. *Chem. Mater.* **2006**, *18*, 5520.

ing phases to vary widely in Li stoichiometry. Consequently, the difference in unit cell volume of the two phases can vary from 4−7%.[5−7] In the absence of misfit dislocations, differential strains of this magnitude must induce a large coherency stress field across the interfaces if both phases coexist in the same crystallite. Therefore, it is necessary to consider elastic strain energy in the diffuse-interface model. Here, the elastic deformation of the particle is characterized by a displacement vector field $\vec{u}(\vec{r})$.

We assume the delithiation of a $LiFePO_4$ particle to proceed uniformly from the surface inward. The lithium concentration c, $FePO_4$ crystallinity η, and displacement vector $\vec{u}$ are therefore functions of the radial coordinate r alone. The nonradial components of $\vec{u}$ vanish under the spherical symmetry, and we may use $u(r)$ to denote the radial displacement.

When a constant electrical potential ϕ is applied to the cathode during electrochemical delithiation/lithiation, the particle is connected to a lithium reservoir (e.g., Li metal negative electrode) that supplies or removes lithium atoms at a fixed chemical potential $\mu_{Li} = -F\phi$ relative to the positive electrode, where F is Faraday's constant. The particle free energy in such an open system needs to be evaluated relative to the lithium reservoir and thus depends on the applied potential. The total free energy of a cathode particle is expressed as a functional of the three scalar fields, $c(r)$, $\eta(r)$, and $u(r)$

$$F_{tot}[c(r),\eta(r),u(r);\phi] = 4\pi r_s^2\gamma(\eta_s) + \int_0^{r_0} 4\pi r^2\left[f_V(c,\eta,T,\phi) + f_{el}(e_{ij},c,\eta) + \frac{\kappa^2}{2}\left(\frac{\partial c}{\partial r}\right)^2 + \frac{\nu^2}{2}\left(\frac{\partial \eta}{\partial r}\right)^2\right] dr \quad (1)$$

The first term on the right side of eq 1 is the contribution of the free surface, and $\gamma(\eta_s)$ is the surface tension, which is anisotropic in detail. The second integral term includes three contributions:

(A) chemical free energy $f_V(c, \eta, T, \phi)$.

(B) elastic strain energy $f(e_{ij}, c, \eta)$.

(C) chemical and structural gradient energies $\kappa^2/2(dc/dr)^2$ and $\nu^2/2(d\eta/dr)^2$.

The formulation of each term in eq 1 and the choices of related parameters are described below.

(A) The chemical free energy density $f_V(c, \eta, T, \phi)$ is a function of c, η, temperature T, and applied electrical potential ϕ. An appropriate model should produce bulk phase behavior that is consistent with experiment. f_V may be modeled by an extended regular solution formulation[24]

$$f_V(c,\eta,T,\varphi) = \{(1-c)f^{FP}(\eta,T) + cf^{LFP}(\eta,T) + RT[c\ln c + (1-c)\ln(1-c)] + W(\eta)c(1-c) + F\phi c\}/V_m \quad (2)$$

where R is the gas constant and V_m is the molar volume of Li_cFePO_4 (taken to be constant at 43.8 cm^3/mol). f^{FP} and f^{LFP} are the molar free energies of stoichiometric $FePO_4$ ($c = 0$) and $LiFePO_4$ ($c = 1$), respectively. They are given a similar expression

$$f^{FP(LFP)}(\eta,T) = f^{FP(LFP),c}(T) + \Delta f^{FP(LFP),c\rightarrow a}(T)p(\eta) + \frac{a^2_{FP(LFP)}(T)}{2}\eta^2(1-\eta)^2 \quad (3)$$

where $p(\eta)$ is a smooth interpolation function between $p(1) = 0$ and $p(0) = 1$

$$p(\eta) = (1-\eta)^3(1+3\eta+6\eta^2) \quad (4)$$

f^{FP} and f^{LFP} as given by eq 3 have a double-well form with two local energy minima at $\eta = 1$ (crystalline) and 0 (amorphous), as illustrated in Figure 1. $f^{FP,c}$ (or $f^{LFP,c}$) in eq 3 is the molar free energy of crystalline $FePO_4$ (or $LiFePO_4$). $\Delta f^{FP,c\rightarrow a} \equiv f^{FP,a} - f^{FP,c}$ is the molar free energy difference between crystalline and amorphous $FePO_4$, and $\Delta f^{LFP,c\rightarrow a} \equiv f^{LFP,a} - f^{LFP,c}$ is the corresponding quantity for $LiFePO_4$. The term $a^2_{FP(LFP)}\eta^2(1-\eta)^2/2$ represents the free energy barrier between bulk crystalline and amorphous $FePO_4$ (or $LiFePO_4$) phases, with the parameter $a^2_{FP(LFP)}$ scaling the barrier height and the crystalline-amorphous $FePO_4$ (or $LiFePO_4$) interface energy.

The regular solution coefficient W in eq 2 characterizes the nonideal interaction of lithium ions with neighboring vacancies and the $FePO_4$ matrix. In general, W takes different values in different structures, e.g., in the solid and liquid forms. Similar to the procedure in ref 24, W is modeled here as a function of the crystallinity of the $FePO_4$ phase

$$W(\eta) = W_c + (W_a - W_c)p(\eta) \quad (5)$$

As illustrated in Figure 1, $W(\eta)$ smoothly interpolates between the regular solution coefficients of crystalline ($\eta = 1$) and amorphous ($\eta = 0$) Li_cFePO_4, i.e., W_c and W_a.

We arrive at reasonable numerical values for the various parameters as follows. At room temperature (e.g., $T = 298$ K), coexistence of olivine $LiFePO_4$ and $FePO_4$ occurs at a potential of $\phi_{coex} = 3.45$ eV (taken relative to Li metal). If choosing olivine $LiFePO_4$ as the reference state, i.e., setting $f^{LFP,c} = 0$, we obtain $f^{FP,c} = -F\phi_{coex} = -332$ kJ/mol. The values of other parameters ($\Delta f^{FP,c\rightarrow a}$, $\Delta f^{LFP,c\rightarrow a}$ and $a^2_{FP(LFP)}$) in eq 3 are not known from experiment, but can be estimated. Although several groups have synthesized hydrated or dehydrated (lithium) iron phosphate glass,[27−33] to the best of our knowledge, the free energy of amorphous $FePO_4$ has not been reported. However, various experimental observations do suggest that $FePO_4$ is a good glass former and that its amorphous phase has a relatively small free energy difference with the crystalline phase. Amorphous $FePO_4$ can be easily obtained upon quenching from the melt[32] or heating amorphous $FePO_4$ hydrates,[27−31] and they remain amorphous upon lithiation[29] or heating to about 500 °C.[27−31,33] It has been found that pressure-induced amorphization of $FePO_4$ occurs at surprisingly low pressures[34] compared to other

(27) Hong, Y. S.; Ryu, K. Y.; Park, Y. J.; Kim, M. G.; Lee, J. M.; Chang, S. H. *J. Mater. Chem.* **2002**, *12*, 1870.
(28) Song, Y.; Yang, S.; Zavalij, P. Y.; Whittingham, M. S. *Mater. Res. Bull.* **2002**, *37*, 1249.
(29) Prosini, P. P.; Lisi, M.; Scaccia, S.; Carewska Cardellini, F.; Pasqualib, M. *J. Electrochem. Soc.* **2002**, *149* (3), A297.
(30) Masquelier, C.; Reale, P.; Wurm, C.; Morcrette, M.; Dupont, L.; Larcher, D. *J. Electrochem. Soc.* **2002**, *149*, A1037.

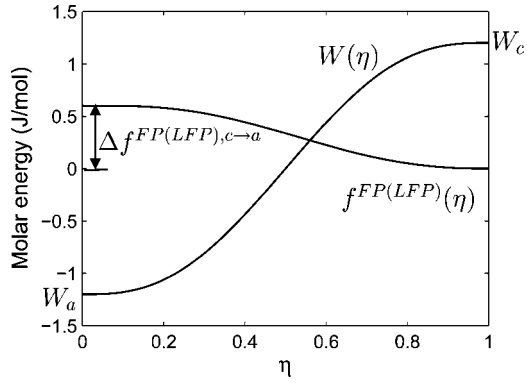

Figure 1. Crystallinity dependence of the molar free energy of stoichiometric $FePO_4$ (or $LiFePO_4$) f^{FP} (or f^{LFP}) and the regular solution coefficient $W(\eta)$ with $\Delta f^{FP(LFP),c\to a} = a^2_{FP(LFP)}/2 = 6$ kJ/mol and $W_c = -W_a = 12$ kJ/mol.

similar structures like SiO_2 and $AlPO_4$. Doping $LiFePO_4$ with Nb was found to promote glass formation of $LiFePO_4$ during melt quenching by Hirose et al.,[33] suggesting that alloying may further reduce the free energy difference between amorphous and crystalline $LiFePO_4$. Guided by available free energy data for crystalline and glassy silica, we assume a relatively small value of 6 kJ/mol for $\Delta f^{FP,c\to a}$ at 298 K. Furthermore, we assume that the difference in molar free energy between crystalline and amorphous phases is the same for both endmember compositions, $\Delta f^{LFP,c\to a} = \Delta f^{FP,c\to a}$. At the equilibrium temperature of bulk crystalline and amorphous stoichiometric $FePO_4$ (or $LiFePO_4$) phases, the crystalline-amorphous interface energy is equal to $a_{FP(LFP)}\nu/(6\sqrt{V_m})$, where ν is the coefficient of the crystallinity gradient energy term. Here, we set $a^2_{FP(LFP)} = 2\Delta f^{FP,c\to a}$. Combined with a choice of $\nu^2 = 1 \times 10^{-11}$J/cm (see subsection C), it gives a crystalline-amorphous interface energy of 0.087 J/m^2, comparable to the silicon-amorphous SiO_2 interface energy of $\sim$0.09J/m^2.[35]

Olivine Li_cFePO_4 with intermediate c values tends to phase-separate into Li-poor and Li-rich phases at room temperature, which suggests a positive regular solution coefficient for the crystalline structure. By fitting the temperature-dependent miscibility data of Dodd et al.,[36] we obtained $W_c = W(\eta = 1) = 12$ kJ/mol. The regular solution coefficient for amorphous Li_cFePO_4, W_a, is less certain, but should be less positive or negative in value since the voltage vs capacity curves for amorphous $FePO_4$, e.g., material derived from iron phosphate hydrates,[29,30] show continuous variation indicating a single solid solution phase at all lithium concentrations. In principle, W_a could be extracted from equilibrium potential−composition curves for the amorphous phase, for instance using galvanostatic intermittent titration (GITT). In the absence of equilibrium data, we fit to several published low C-rate galvanostatic charge/discharge curves for hydrated amorphous Li_cFePO_4[29,30] and obtained values ranging from −20 to −40 kJ/mol. These are likely to be more negative than the true values (because state-of-charge dependent polarization often increases the slope of galvanostatic potential curves), so for the model we set $W_a = W(\eta = 0) = -W_c$.

Figure 2a shows the volume free energy surface at $T = 298$ K specified by eq 1 using the parameter values chosen above. The free energy curves of the crystalline and amorphous states, i.e., the cross-sections of the free energy surface at $\eta = 1$ and 0, are shown in Figure 2b. To facilitate viewing, a linear portion of the free energy, $\mu_{coex}c$, has been subtracted from the plotted free energy surface and curves (this subtraction has no effect on the determination of limiting compositions in the two phase regions), where $\mu_{coex} = -332$ kJ (or $\phi_{coex} = 3.45$ eV) is the equilibrium lithium chemical potential at the coexistence of olivine $LiFePO_4$ and $FePO_4$. With the chosen parameter values crystalline Li_cFePO_4 displays a symmetric free energy curve, and lithium has a solubility of $c_0 = 0.85\%$ and $(1 - c_0) = 99.15\%$ in the Li-poor and Li-rich phases, respectively. These solid solution limits are close to those observed experimentally for coarse bulk phases.[5,6,37] To simplify notation we will continue to refer to the nonstoichiometric delithiated and lithiated phases as $FePO_4$ and $LiFePO_4$. Using this model, the free energy of amorphous Li_cFePO_4 lies well above that of the crystalline phase at 298K, Figure 2b. Applying the common tangent construction to the free energy curves in Figure 2b, one finds that the olivine $LiFePO_4$ and amorphous Li_cFePO_4 phases could coexist at $\mu_{Li} = \mu_{coex} - 2.501$ kJ/mol. However, this chemical potential is lower than the equilibrium potential for the coexistence of crystalline $LiFePO_4$ and $FePO_4$, μ_{coex}. A bulk phase transition from the olivine $LiFePO_4$ to the amorphous Li_cFePO_4 would be preceded by the crystalline transition upon delithiation and is not thermodynamically permitted in the bulk form, consistent with experimental experience.

(B) The elastic energy density $f_{el}(e_{ij}, c, \eta)$ at small strains can be generally written as

$$f_{el} = \frac{1}{2}C_{ijkl}(e_{ij} - e^0_{ij})(e_{kl} - e^0_{kl}) \quad (6)$$

where C_{ijkl} is the elastic stiffness tensor and e_{ij} the elastic strain tensor. Given the spherical symmetry of the displacement field $u(\vec{r})$, the only nonzero components of the elastic strain tensor are e_{rr}, $e_{\theta\theta}$, and $e_{\phi\phi}$, which are related to the radial displacement u as

$$e_{rr} = \frac{du}{dr} \quad (7)$$

(31) Okada, S.; Yamamoto, T.; Okazaki, Y.; Yamaki, J.; Tokunaga, M.; Nishida, T. *J. Power Sources* **2005**, *146*, 570.
(32) Friebele, E. J.; Wilson, L. K.; Dozier, A. K.; Kinser, D. L. *Phys. Status Solidi A* **1971**, *45*, 323.
(33) Hirose, K.; Honma, T.; Benino, Y.; Komatsu, T. *Solid State Ionics* **2007**, *178*, 801.
(34) Pasternak, M. P.; Rozenberg, G. Kh.; Milner, A. P.; Amanowicz, M.; Zhou, T.; Schwarz, U.; Syassen, K.; Dean Taylor, R.; Hanfland, M.; Brister, K. *Phys. Rev. Lett.* **1997**, *79*, 4409.
(35) Patel, J. R. *Semiconductor Silicon 1981*; Huff, H. R., Kriegler, R. J., Takeishi, Y., Eds.; Electrochemical Society: Pennington, NJ, 1981; p189.
(36) Dodd, J. L.; Yazami, R.; Fultz, B. *Electrochem. Solid-State Lett.* **2006**, *9*, A151.
(37) Yamada, A.; Koizumi, H.; Sonoyama, N.; Kanno, R. *Electrochem. Solid-State Lett.* **2005**, *8*, A409.
(38) Delcourt, C.; Poizot, P.; Tarascon, J.-M.; Masquelier, C. *Nat. Mater.* **2005**, *4*, 254.

$$e_{\theta\theta} = e_{\phi\phi} = \frac{u(r)}{r} \tag{8}$$

In eq 6, e_{ij}^0 is the stress-free strain tensor and defined as the relative difference of the local lattice parameter from a reference state, selected to be olivine $LiFePO_4$. With the isotropic approximation, eq 6 becomes

$$f_{el} = \left(\frac{K}{2} - \frac{G}{3}\right)\left(\frac{du}{dr} + 2\frac{u}{r} - 3e^0\right)^2 + G\left(\frac{du}{dr} - e^0\right)^2 + 2G\left(\frac{u}{r} - e^0\right)^2 \tag{9}$$

where e^0, K, and G are the stress-free strain, bulk, and shear moduli of Li_cFePO_4 averaged over crystallographic orientations, respectively. e^0 is a function of the local lithium concentration in the crystalline state, and is zero by definition for $LiFePO_4$, i.e., $e^0(c = 1 - c_0) = 0$. Because experimental data show that the lattice parameters of olivine Li_cFePO_4 exhibit a linear dependence on lithium concentration (Vegard's law),[38] we have

$$e^0(c) = \Delta e^0\left[\frac{c + c_0 - 1}{1 - 2c_0}\right] \tag{10}$$

where $-\Delta e^0$ is the stress-free strain of crystalline $FePO_4$ relative to $LiFePO_4$.

If an amorphous phase forms upon delithiation, its interface with crystalline $LiFePO_4$ is incoherent in nature and thus any coherency stress induced energy in the particle will be small. Strictly speaking, the elastic energy formulation eq 9 is not applicable to such a case. We may, however, approximate the elastic energy if the amorphous phase is assumed to relax to zero "effective" stress-free strain, regardless of its lithium concentration, i.e. $e^0(c, \eta = 0) = 0$. Furthermore, e^0 is defined for states with intermediate crystallinity values between $\eta = 0$ and 1 by interpolation between $e^0(\eta = 1)$ and $e^0(\eta = 0)$

$$e^0 = \Delta e^0\left[\frac{c + c_0 - 1}{1 - 2c_0}\right]p(1 - \eta) \tag{11}$$

This result applies to cases where there is negligible strain energy across the interface between crystalline $LiFePO_4$ and the amorphous phase because the latter has relaxed its structure to achieve a stress free state.

The elastic properties of olivine Li_cFePO_4 have been calculated from first-principles by Maxisch and Ceder.[39] Their GGA+U calculation results of the orientation-averaged bulk and shear moduli of $LiFePO_4$, $K = 93.9$ GPa and $G = 48.4$ GPa, were used as inputs to eq 9. The difference in unit cell volume between $LiFePO_4$ and $FePO_4$ is 4−7% depending on crystallite size and composition,[5−7] which corresponds to an averaged linear misfit strain of 1−2%. Thus Δe^0 is correspondingly varied from 0 to 0.02 to study the effect of misfit strain on Li_cFePO_4 phase transition behavior, presented later.

(C) The gradient energy densities, $\kappa^2/2(dc/dr)^2$ and $\nu^2/2(d\eta/dr)^2$, arise from the spatial variations of lithium concentration and crystallinity within the particle. The term $\kappa^2/2(dc/dr)^2$ contributes to the interface energy between lithiated and delithiated phases, whereas $\nu^2/2(d\eta/dr)^2$ is related to the interface energy between amorphous and crystalline phases. Experimental values of the gradient coefficients κ^2 and ν^2 are not available for Li_cFePO_4. The values $\kappa^2 = 5 \times 10^{-12}$ J/cm and $\nu^2 = 1 \times 10^{-11}$J/cm were adopted in our model calculations; these are comparable to those used for other systems such as Si_3N_4.[40]

In eq 1, the particle surface energy $4\pi r_s^2\gamma(\eta_s)$ depends on the actual particle radius, $r_s = r_0 + u(r_0)$, and the surface crystallinity, $\eta_s = \eta(r_0)$. This term consists of both surface tension and surface stress. For small strains r_s^2 can be approximated by $r_0^2(1 + 2u(r_0)/r_0)$. The surface tension of Li_cFePO_4, γ, is treated as isotropic and independent of Li concentration in the model, although this is not strictly correct.[41,42] Because crystalline and amorphous phases differ in their surface energies, γ is a function of crystallinity. Here we approximate $\gamma(\eta)$ with the leading terms of its series expansion with respect to η

$$\gamma = \gamma_a + \Delta\gamma\eta^2 \tag{12}$$

where γ_a is the surface tension of the amorphous phase and $\Delta\gamma(>0)$ is the surface tension difference between crystalline and amorphous phases. The absolute magnitude of γ_a is not important because we will use only the energy difference. In the absence of data for the surface energy of amorphous Li_cFePO_4, we assume a value $\Delta\gamma = 0.2$ J/m^2, comparable to that of SiO_2.[43]

For the particle energy F_{tot}, eq 1, we seek mathematical solutions of $c(r)$, $\eta(r)$, and $u(r)$ that represent locally stable particle states, or the minimal energy barriers between them. Such solutions should be extrema of F_{tot}, i.e., $\delta F_{tot}[c(r), \eta(r), u(r)] = 0$; they should satisfy the Euler equations

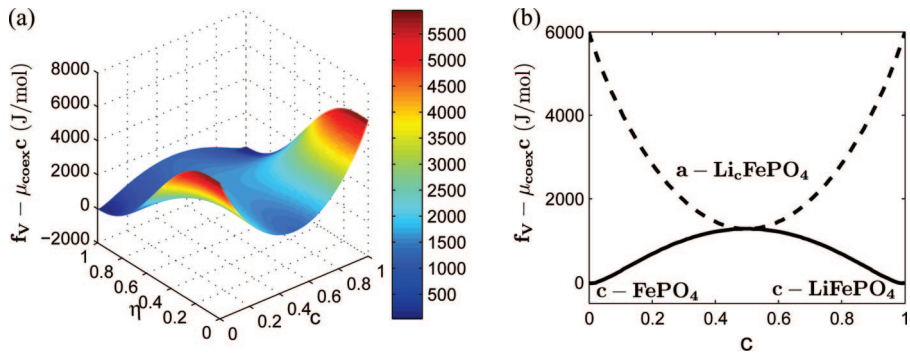

Figure 2. (a) Model free energy surface of Li_cFePO_4 at $T = 298$ K. (b) Free energy curves of crystalline and amorphous Li_cFePO_4 at $T = 298$ K.

$$\kappa^2\left(\frac{d^2c}{dr^2} + \frac{2}{r}\frac{dc}{dr}\right) + 3K\frac{\partial e^0}{\partial c}\left(\frac{du}{dr} + 2\frac{u}{r} - 3e^0\right) - \frac{\partial f_V}{\partial c} = 0 \quad (\delta F_{tot}/\delta c(r) = 0) \quad (13)$$

$$\nu^2\left(\frac{d^2\eta}{dr^2} + \frac{2}{r}\frac{d\eta}{dr}\right) + 3K\frac{\partial e^0}{\partial \eta}\left(\frac{du}{dr} + 2\frac{u}{r} - 3e^0\right) - \frac{\partial f_V}{\partial \eta} = 0 \quad (\delta F_{tot}/\delta \eta(r) = 0) \quad (14)$$

$$\frac{d^2u}{dr^2} + \frac{2}{r}\frac{du}{dr} - \frac{2}{r^2}u - \frac{9K}{3K + 4G}\left(\frac{\partial e^0}{\partial c}\frac{dc}{dr} + \frac{\partial e^0}{\partial \eta}\frac{d\eta}{dr}\right) = 0 \quad (\delta F_{tot}/\delta u(r) = 0) \quad (15)$$

Note that eq 15 represents the condition of mechanical equilibrium within the particle and can also be directly derived from the general stress equilibrium equations. In addition to eqs 13−15, $c(r)$, $\eta(r)$, and $u(r)$ should also meet the following boundary conditions

$$\frac{dc}{dr}|_{r=0} = 0 \quad (16)$$

$$\frac{d\eta}{dr}|_{r=0} = 0 \quad (17)$$

$$u(r = 0) = 0 \quad (18)$$

$$\frac{dc}{dr}|_{r=r_0} = 0 \quad (19)$$

$$\left[\nu^2\frac{d\eta}{dr} + \left(1 + 2\frac{u(r_0)}{r_0}\right)\frac{d\gamma}{d\eta}\right]\Bigg|_{r=r_0} = 0 \quad (20)$$

$$\left(K + \frac{4}{3}G\right)\frac{du}{dr}\Bigg|_{r=r_0} + \left(2K - \frac{4}{3}G\right)\frac{u(r_0)}{r_0} - 3Ke^0(c(r_0), \eta(r_0)) + \frac{2}{r_0}\gamma(\eta(r_0)) = 0 \quad (21)$$

Equations 13−21 were solved numerically for the spatially varying composition, crystallinity, and strain fields within particles under conditions of interest. We also examined the stability of obtained solutions by applying a functional gradient descent method, as described in the Appendix.

3. Results and Discussion

3.1. Stable Bulk and Surficial Phase Configurations Obtained from Solutions to the Diffuse-Interface Model. We begin by presenting three locally stable solutions of eqs 13−21, each corresponding to the spatially varying composition, crystallinity, and strain within a particle under conditions where the entire particle is one of the three possible bulk phases: crystalline $LiFePO_4$ (cLFP), crystalline $FePO_4$ (cFP), and amorphous Li_cFePO_4 solid solution (aFP). Figure 3a−c shows the lithium concentration, crystallinity, and displacement fields within a 100 nm diameter particle of each phase, respectively. A zero misfit strain ($\Delta e^0 = 0$) is used in the calculations shown here. During the delithiation (charging) process, the crystalline $FePO_4$ particle has the lowest free energy of the three bulk phases when the lithium chemical potential is below μ_{coex}. This corresponds to a positive applied overpotential, $\Delta\phi = \phi - \phi_{coex}$. A phase transition from one of the other phases to crystalline $FePO_4$ is thermodynamically favorable at $\Delta\phi > 0$. However, as described in the next section, such transitions need to overcome energy barriers (or activation energies) and a particle can remain in the crystalline $LiFePO_4$ or amorphous Li_cFePO_4 phase as a metastable state at $\Delta\phi > 0$. The solutions for crystalline phases cLFP and cFP, panels a and b in Figure 3, show appreciable structural disorder near the particle surface due to the reduction in surface energy for low surface crystallinity, as well as a slight variation in lithium concentration at the surface. Thus the model predicts deviations in surface structure and composition even in predominantly single-phase crystalline particles. Only the amorphous particle (Figure 3c), which has the lowest surface energy, has uniform composition.

At sufficiently large overpotentials, another locally stable mathematical solution is found, corresponding to the unique state referred to earlier of a surficial amorphous film (SAF). This solution, labeled saLFP in Figure 3d, has the lithium concentration and crystallinity of cLFP in the particle interior, but has a stable nanometer-thick surface region with much greater structural disorder and lower lithium concentration than the underlying crystal. The surface region still possesses a finite degree of crystallinity, and as with other SAFs, it is not simply a thin layer of a bulk amorphous phase, but is an equilibrium feature under the imposed thermodynamic conditions. For example, there is an "equilibrium thickness" to the disordered surficial phase at a given value of temperature, pressure, and overpotential. Other inorganic systems exhibit similar disordered surface structures of stable nanoscale thicknesses.[14,15] Reviews of the SAF phenomenon can be found in refs 16 and 17. In the present case, the implication of the results is that a bulk phase transition occurring during delithiation may be preceded by a surface phase transition, between the state cLFP (Figure 3a) and the state saLFP (Figure 3d). Thus the saLFP state is an intermediate state along the transition pathway to a single-phase particle or some other multiphase state.

3.2. Critical Nucleus Configurations for the Phase Transformations, Represented by Unstable Solutions of the Diffuse-Interface Model. The previous section discussed stable solutions to the model corresponding to the locally stable states in which a particle may dwell. Transitions between the various stable states will typically be subject to an energy barrier that is equal to the free energy of the critical nucleus. In the diffuse-interface model, the critical nucleus is not a size-dependent quantity as in simple nucleation theory, but is a state of the particle having a particular distribution of composition, order, and displacement, through which particles must pass as they evolve from one stable phase to another. The energy of a critical nucleus state can be obtained from the unstable

(39) Maxisch, T.; Ceder, G. *Phys. Rev. B* **2006**, *73*, 174112.
(40) Bishop, C. M.; Cannon, R. M.; Carter, W. C. *Acta Mater.* **2005**, *53*, 4755.
(41) Wang, L.; Zhou, F.; Meng, Y. S.; Ceder, G. *Phys. Rev. B* **2007**, *76*, 165435.
(42) Fisher, C. A. J.; Islam, I. S. *J. Mater. Chem.* **2008**, *18*, 1209.
(43) Parks, G. A. *Rev. Mineral.* **1990**, *23*, 133.

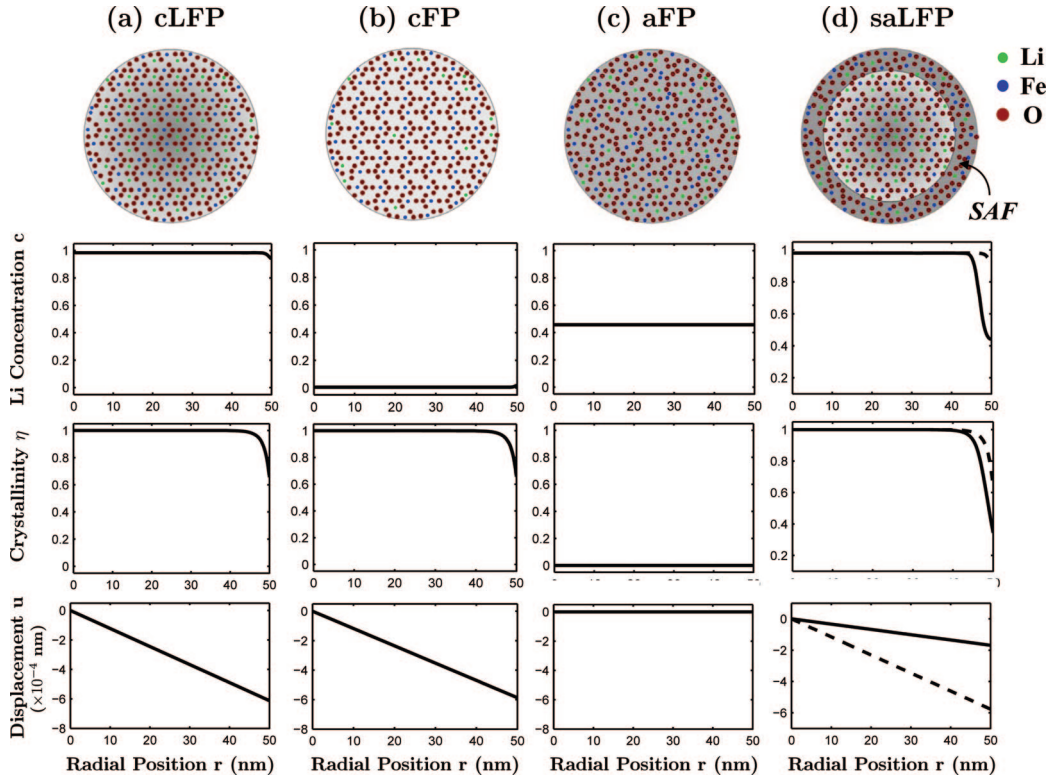

Figure 3. Radial distributions of the lithium concentration $c(r)$, crystallinity $\eta(r)$, and displacement $u(r)$ in a 100 nm diameter particle, corresponding to local minima of the energy functional F_{tot} in the diffuse-interface model and conditions where the bulk phase is (a) crystalline $LiFePO_4$, cLFP; (b) crystalline $FePO_4$, cFP; (c) amorphous, partially lithiated Li_cFePO_4, aFP. Distributions a−c are obtained at an overpotential of $\Delta\phi = 15$ mV. (d) Solution obtained for a crystalline $LiFePO_4$ particle at a larger overpotential, $\Delta\phi = 19.5$mV. Here, a new phase state consisting of a surficial amorphous film (SAF) on a crystalline $LiFePO_4$ core is locally stable. The dashed lines correspond to cLFP at the same overpotential when the SAF is not permitted. Schematic illustrations of composition and atomic order within the particles are shown at top.

Table 1. List of Model Parameters

parameters	physical meaning	values
V_m	molar volume of Li_cFePO_4	43.8 cm^3/mol
$\Delta f^{FP,c\rightarrow a}$	volumetric free energy density difference between crystalline and amorphous $FePO_4$	6 kJ/mol[a]
$\Delta f^{LFP,c\rightarrow a}$	volumetric free energy density difference between crystalline and amorphous $LiFePO_4$	6 kJ/mol[a]
$a^2_{FP(LFP)}$	free energy barrier between crystalline and amorphous $FePO_4$ ($LiFePO_4$)	12 kJ/mol[a]
W_c	regular solution coefficient of crystalline Li_cFePO_4	12 kJ/mol
W_a	regular solution coefficient of amorphous Li_cFePO_4	−12 kJ/mol
K	orientation-averaged bulk modulus	93.9 GPa
G	orientation-averaged shear modulus	48.4 GPa
Δe^0	misfit strain between lithiated and delithiated olivines	0−0.02
κ^2	chemical gradient coefficient	5×10^{-12} J/cm[a]
ν^2	crystallinity gradient coefficient	1×10^{-11} J/cm[a]
$\Delta\gamma$	surface tension difference between crystalline and amorphous Li_cFePO_4	0.2 J/m^2[a]

[a] Estimated values using silica and silicon nitride data as guidance.

Table 2. List of the Stable and Unstable Solutions of eqs 13−21

solution name	physical meaning
cLFP	particle in crystalline $LiFePO_4$ bulk phase
cFP	particle in crystalline $FePO_4$ bulk phase
aFP	particle in amorphous Li_cFePO_4 phase
saLFP	crystalline $LiFePO_4$ particle with a surficial amorphous film (SAF)
cn-cFP	critical nucleus state for crystalline phase transition cLFP → cFP
cn-aFP	critical nucleus state for the amorphous phase transition cLFP → aFP
cn-saLFP	critical nucleus state for surficial phase transition cLFP → saLFP
max-FP	locally maximal energy barrier for phase transitions from cLFP to cFP or aFP

solutions to eqs 13−21. This section discusses the physical configurations of these critical nucleus states for the transformation of an initially crystalline $LiFePO_4$ particle to other phase states. The magnitude of the activation barrier and its dependence on particle size and overpotential are presented in the following section.

Each of the several possible transition pathways from crystalline $LiFePO_4$ to other bulk or surficial phases has a unique mathematical solution, or critical nucleus state. Table 2 lists the labels for various mathematical solutions and their physical meaning. These solutions are plotted in Figure 4a−c for a 100 nm-diameter particle. The instability of these solutions, which identify them as energy barriers along a transition pathway, was established using the functional gradient descent minimization described in the Appendix. There it is shown that each of such solutions can continuously evolve toward two "nearby" locally stable by a continuous decrease in total free energy. Figure 4a shows the $c(r)$, $\eta(r)$, and $u(r)$ profiles corresponding to the critical nucleus state

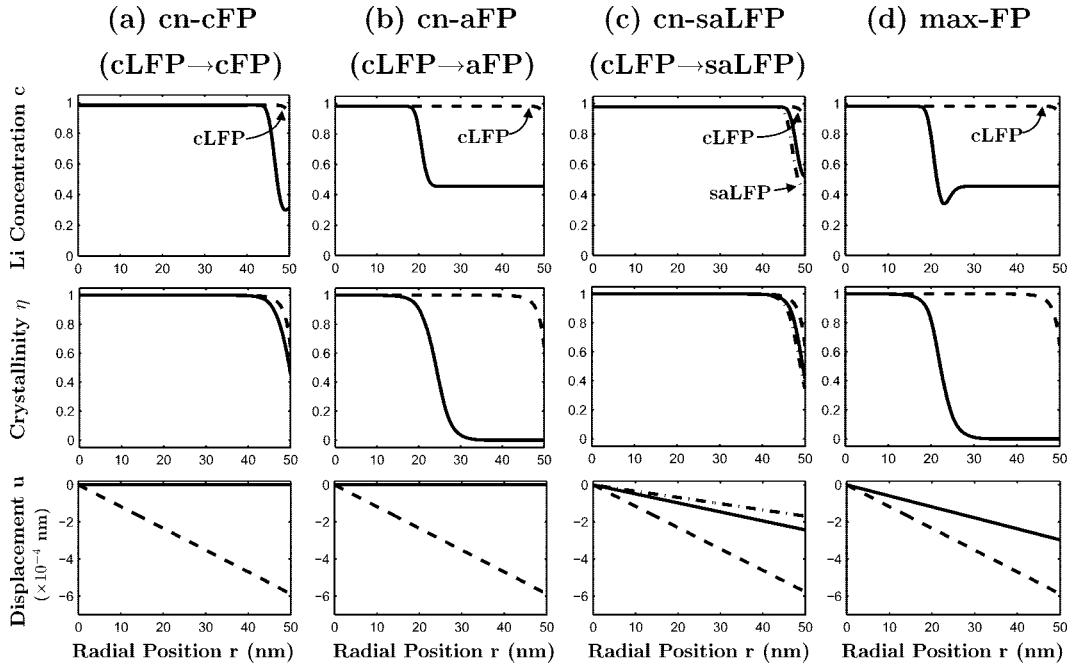

Figure 4. Along any thermally activated transition pathway there exists a critical nucleus state and an associated energy barrier, obtained from unstable solutions to eqs 13−21. Here the critical nucleus configurations associated with various phase transitions of an initially crystalline $LiFePO_4$ particle are shown: (a) cn-cFP, the critical nucleus state for the crystalline phase transition cLFP → cFP that represents the minimal energy barrier for such a transition. (b) cn-aFP, the critical nucleus state for the amorphous phase transition cLFP → aFP that represents the minimal energy barrier for this transition. (c) cn-saLFP, the critical nucleus for the surficial phase transition cLFP → saLFP that is the minimal energy barrier for the transition. (d) max-FP corresponds to a locally maximal energy barrier for bulk phase transitions cLFP → cFP or cLFP → aFP. The radial distributions of $c(r)$, $\eta(r)$, and $u(r)$ of these energy barriers are shown for a 100 nm diameter particle at $\Delta\phi = 15$ mV for a, b, and d and at $\Delta\phi = 19.5$ mV for c. For comparison, the starting phase cLFP of the transitions is also plotted as dashed lines in a−d, and saLFP as the dash-dotted line in c.

for the "conventional" phase transition from crystalline $LiFePO_4$ to crystalline $FePO_4$, abbreviated as "cn-cFP." The dashed lines show the results from the stable solution (locally stable phase state). When the Li concentration, crystallinity, and displacement fields of the olivine $LiFePO_4$ particle are each perturbed (e.g., by thermal fluctuation) and reach beyond the $c(r)$, $\eta(r)$, and $u(r)$ profiles shown for cn-cFP, the perturbation will grow with time and transform the entire particle into the delithiated crystalline $FePO_4$ phase; otherwise the particle remains stable against the transition. On the particle free energy landscape, cn-cFP corresponds to a saddle point energy between two local energy minima of F_{tot} corresponding to the phases cLFP and cFP. Its free energy excess compared to cLFP is the minimal energy barrier a particle needs to overcome for the cLFP → cFP transition to occur; other phase transformation pathways are also possible but have higher energy barriers. These results correspond to the case where the phase transition starts from the particle surface and progresses inward.

A second solution, cn-aFP in Figure 4(b), represents the critical nucleus state for the transition of crystalline $LiFePO_4$ to amorphous Li_cFePO_4 (cLFP → aFP). As above, the energy difference between the critical nucleus state and the starting phase cLFP is the minimal energy barrier associated with amorphization of the initially crystalline particle. Figure 4(c) shows a third solution, corresponding to conditions such as high overpotentials where a surficial amorphous film (SAF) on crystalline $LiFePO_4$ is a locally stable configuration. The energy difference between this solution and cLFP gives the minimal energy barrier for a surficial phase transition to form an SAF on a crystalline $LiFePO_4$ particle. In Figure 4c, dashed lines show the beginning (cLFP) and end (saLFP) states as well.

Figure 4d shows another unstable solution of eqs 13−21, max-FP, that has a different significance from the three critical nucleus solutions above. This solution does not represent a saddle point between cLFP and other local minima of F_{tot} or bear the physical significance of a minimal transition energy barrier, but is a maximal point of F_{tot} corresponding to a locally maximal energy barrier for transitions from crystalline $LiFePO_4$ to crystalline or amorphous $FePO_4$. The relevance of this solution to phase transition pathways will be discussed in more detail in the next section.

3.3. Effects of Particle Size and Overpotential on Phase Transition Behavior. The solutions for the critical nuclei in the previous section each describe a different phase transition pathway a crystalline $LiFePO_4$ can undergo during delithiation. Each pathway has an energy barrier (activation energy), ΔF, which is the free energy difference between the critical nucleus state and the initially crystalline $LiFePO_4$ phase. Comparing the activation energies of the various crystalline and amorphous phase transitions, and how these energies are affected by experimentally relevant parameters, allows evaluation of the probability of the thermally activated transition, which is proportional to $\exp(-\Delta F/kT)$. Two physical parameters are the particle size and misfit strain between the lithiated and delithiated olivine. Another parameter that has not been emphasized in previous literature

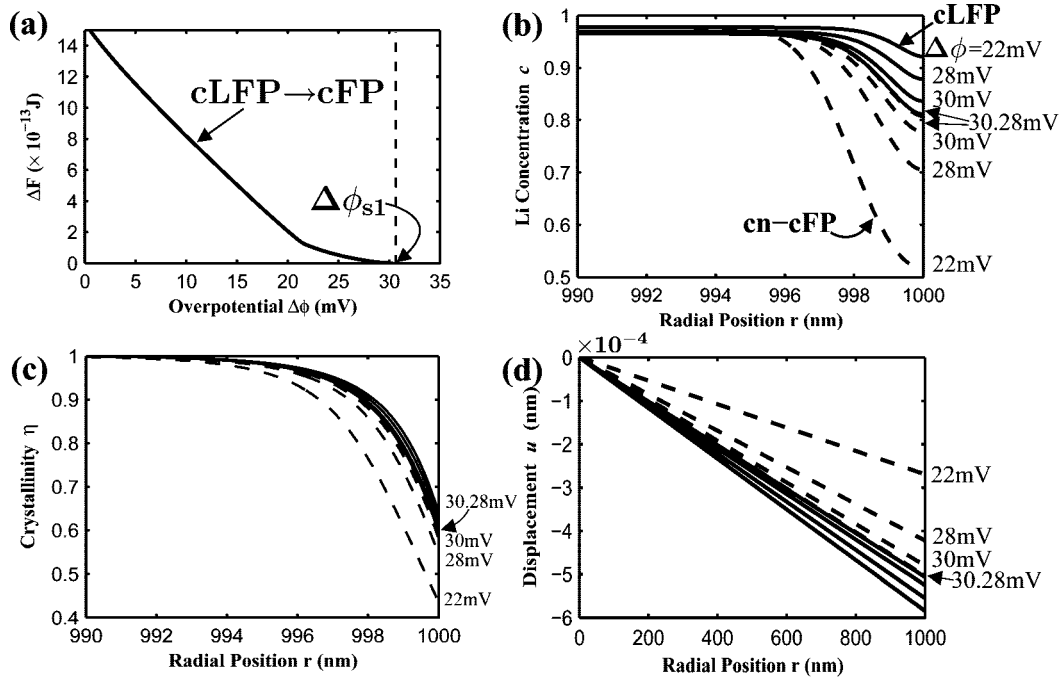

Figure 5. (a) Overpotential dependence of the activation energy, $\Delta F = F_{tot}$(cn-cFP) − F_{tot}(cLFP), for transformation of a large particle (here, $r_0 = 1$ μm) of crystalline $LiFePO_4$ (cLFP) to crystalline $FePO_4$ (cFP) with increasing overpotential, $\Delta\phi$. The activation energy decreases with increasing overpotential and evolves toward zero at a critical overpotential $\Delta\phi_{s1} = 30.283$ mV. Above this overpotential, the phase transformation is barrierless and occurs spontaneously. (b−d) $c(r)$, $\eta(r)$, and $u(r)$ profiles for cLFP (solid lines) and cn-cFP (dashed lines). Solutions are shown for $\Delta\phi = 22$, 28, 30, and 30.28 mV. The two mathematical solutions cLFP and cn-cFP approach each other as $\Delta\phi \rightarrow \Delta\phi_{s1} = 30.283$ mV, indicating a barrierless phase transition.

but potentially has a large influence on the transition energy barriers is the overpotential, which affects lithium chemical potential through the chemical free energy density, see eq 2. The overpotential $\Delta\phi$ is perhaps the most easily controlled, and widely varied, experimental parameter. The effects of overpotential and particle size on the phase transition pathway are coupled. To make the results more transparent, we first "turned off" the elastic strain energy (by setting the misfit strain to zero, $\Delta e^0 = 0$). The misfit strain effects are then added in section IV.

Results for 2 μm Particle Diameter. At relatively large particle sizes, e.g., $r_0 = 1$ μm, it was found that the direct phase transition to crystalline $FePO_4$ is the only possible transition pathway in the absence of strain. The critical nucleus that is required for the minimum-energy amorphization pathway, cn-aFP, is much larger than that for the crystalline transformation pathway, cn-cFP. However, the activation energy for the preferred crystalline transformation cLFP → cFP, given by the energy difference between cn-cFP and cLFP and denoted $\Delta F_{c\rightarrow c}$, is lowered by increasing the overpotential $\Delta\phi$, and eventually reaches zero at $\Delta\phi_{s1} = 30.283$ mV as shown in Figure 5a. This behavior may be understood as follows. At zero overpotential the activation energy for transformation of the $r_0 = 1$ μm particle is $\sim 1.6 \times 10^{-12}$ J, corresponding to a molar energy of 17 J/mol. With increasing overpotential, the activation energy initially decreases in a nearly linear manner because of the dependence of chemical free energy on electrical potential (eq 2). As the overpotential increases further, the stable state of the cLFP phase includes an increasingly disordered and delithiated surface, shown by the solid lines at increasing overpotential in panels b and c in Figure 5. The $c(r)$, $\eta(r)$, and $u(r)$ profiles for the critical nucleus as a function of overpotential are also shown in Figure 5b−d as dashed lines. These curves show that the state of the crystalline cLFP particle (solid lines) and the state of the critical nucleus for transformation to crystalline cFP, cn-cFP (dashed lines), approach one another as the overpotential increases. At a critical overpotential $\Delta\phi_{s1} = 30.283$ mV, the two curves converge, and the transformation from cLFP to cFP becomes barrierless and the transformation becomes spontaneous. A crystalline $LiFePO_4$ particle becomes unstable against arbitrarily small thermal fluctuation and will spontaneously transform into the delithiated olivine phase. This remains true for all $\Delta\phi > \Delta\phi_{s1}$, because the local minimum cLFP and the saddle point cn-cFP merge at $\Delta\phi_{s1}$ and these two extrema of F_{tot} disappear at higher overpotentials, meaning neither cLFP nor cn-cFP can be found at $\Delta\phi > \Delta\phi_{s1}$. To summarize this result, an olivine $LiFePO_4$ particle of large particle size will transform to crystalline $FePO_4$ either by thermal activation below a critical potential, $\Delta\phi < \Delta\phi_{s1}$, or by a spontaneous transition above the critical potential, $\Delta\phi > \Delta\phi_{s1}$.

Results for 80 nm Particle Diameter. As the particle size decreases to the nanoscale regime, the phase transition behavior changes to include alternative pathways involving a surface amorphous phase. At 80 nm particle diameter, the stable configurations of the particles are similar to those shown in Figure 3 for a 100 nm diameter particle. In particular, at large enough overpotential, the crystalline $LiFePO_4$ particle may form a surficial amorphous film (SAF) as a metastable configuration. Results for the activation energy of various transition pathways are shown in Figure 6 for a particle diameter of 80 nm.

Figure 6b shows the overpotential dependence of the activation energy for direct crystalline transformation, cLFP

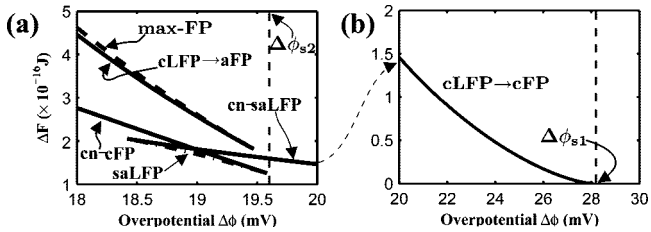

Figure 6. Overpotential dependence of the energy barrier, ΔF, for transformation of an initially crystalline $LiFePO_4$ particle to crystalline and amorphous delithiated end states by various transformation pathways, for a particle of $r_0 = 40$ nm. (a) A crystalline (cLFP) particle with a surficial amorphous film (SAF) becomes unstable against spontaneous transition to crystalline $FePO_4$ at $\Delta\phi_{s2} = 19.58$mV, whereas (b) one without an SAF becomes unstable at a higher overpotential of $\Delta\phi_{s1} = 28.08$ mV. Note the energies for the cn-cFP, cn-saLFP, and saLFP transitions in a are scaled relative to the energy of the crystalline particle cLFP.

→ cFP, which is qualitatively similar to Figure 5a. There is again a critical overpotential, $\Delta\phi_{s1} = 28.08$ mV, above which a crystalline $LiFePO_4$ particle undergoes a barrierless ($\Delta F = 0$) transition to crystalline $FePO_4$, but the critical overpotential is smaller than in Figure 5a because of the smaller particle size. However, an alternative to the direct crystalline transformation exists, in which the SAF is an intermediate state. Figure 6a shows behavior at lower overpotential than in Figure 6b. The lower curves are mathematical solutions of eqs 13−21 for the SAF state (saLFP) and its critical nucleus state (cn-saLFP). These appear for overpotentials above $\Delta\phi = 18.42$mV. The energy barrier to transform a crystalline $LiFePO_4$ particle with an SAF to crystalline $FePO_4$ is given by the energy difference between the critical nucleus states cn-cFP and saLFP, i.e., the gap between the two corresponding curves shown in Figure 6a, which disappears at $\Delta\phi_{s2} = 19.58$mV (Figure 6a)). Note that the saLFP curve in Figure 6a lies at higher energy ΔF ($>1 \times 10^{-16}$ J) than cFP. Formation of the SAF is therefore thermally activated. However, if the SAF is able to form, there arises a new critical overpotential, $\Delta\phi_{s2}$, above which an olivine $LiFePO_4$ particle with SAF will spontaneously transform to crystalline $FePO_4$. In comparison, there still exists a finite energy barrier for the purely crystalline transition, cLFP → cFP, for overpotentials $\Delta\phi \geq \Delta\phi_{s2}$. This energy barrier does not reach zero until the higher critical overpotential, $\Delta\phi_{s1,}$ is reached (Figure 6b). The results in Figure 6 show that a particle with an SAF undergoes a barrierless transition at a lower overpotential than a particle without an SAF. Therefore, formation of an SAF provides a pathway of lower activation energy for the transformation to crystalline $FePO_4$.

The upper lines in Figure 6a) show the activation energy for the transition of the crystalline particle to a bulk amorphous phase. Although the bulk crystalline to amorphous transition, cLFP → aFP, is energetically possible at $\Delta\phi > 17.89$ mV, where the amorphous phase particle has a lower free energy than the crystalline $LiFePO_4$ phase, the energy barrier for such a transition, $\Delta F_{c\to a}$, is larger than that for the crystalline transition, cLFP → cFP (Figure 6b), at any positive overpotential. Thus, it is unlikely that complete amorphization would occur during delithation at this particle size.

In summary, for a particle of 80 nm diameter, transition of an initially crystalline particle to a bulk disordered phase upon delithiation is still unlikely. However, the transition to a crystalline delithiated phase may be preceded by the formation of a surficial amorphous film.

Results for 50 nm Particle Diameter. Remarkable changes in behavior are seen when the particle diameter is further reduced to 50 nm. Although the crystalline $FePO_4$ phase remains more stable than the amorphous phase at $\Delta\phi \geq 0$, as shown in Figure 7a, the activation energy $\Delta F_{c\to a}$ (curve labeled cLFP → aFP) for the transformation of crystalline $LiFePO_4$ directly to amorphous $FePO_4$ now becomes comparable to the energy $\Delta F_{c\to c}$ (curve labeled cLFP → cFP) for the crystalline-to-crystalline transition. Although at small overpotentials $\Delta F_{c\to a}$ is still larger than $\Delta F_{c\to c}$, the former decreases more rapidly with increasing $\Delta\phi$. A crossover between the two energy barriers occurs at a critical overpotential $\Delta\phi_e = 11.21$ mV, above which the amorphization pathway has the smaller activation energy. Figure 7a also shows that the cLFP → cFP curve meets the maximal energy barrier curve, max-FP, at $\Delta\phi = 15.8$ mV, and neither cn-cFP nor max-FP are found at higher overpotentials. This does not imply that there is no energy barrier associated with the crytalline transition cLFP → cFP above $\Delta\phi = 15.8$ mV; it rather suggests that attaining a minimal energy barrier for such a transition requires a two-step process: the crystalline $LiFePO_4$ particle will amorphize first followed by a second transition aFP → cFP to reach the final state crystalline $FePO_4$. In other words, the amorphous phase must be involved as an intermediate state along the transition pathway.

Figure 7b shows the same results but at a higher range of overpotentials than in Figure 7a. Now, the transformation from crystalline $LiFePO_4$ to amorphous $FePO_4$ may occur through an intermediate state where there is a surficial phase saLFP on a cLFP particle, the energy barrier for which is again represented by the energy difference between the solutions cn-cFP and saLFP. As in the case of the 80 nm particle, the SAF does not form spontaneously but requires thermal activation. Once formed, however, it provides a lower activation energy pathway to bulk amorphization. This is seen in the values of the critical overpotentials in b and c in Figure 7, respectively. The amorphization energy barriers for a cLFP particle with and without SAF both decrease with increasing overpotential, and they approach zero at $\Delta\phi_{s2} = 16.43$mV (Figure 7b) and $\Delta\phi_{s1} = 26.56$ mV (Figure 7c), respectively. Similar to the 80 nm diameter particle, a 50 nm diameter crystalline $LiFePO_4$ particle also becomes unstable at one of the two characteristic overpotentials, $\Delta\phi_{s1}$ and $\Delta\phi_{s2}$, depending on its surface state. However, the key difference is that the 50 nm particle will spontaneously amorphize at these overpotentials instead of undergoing a barrierless cLFP → cFP crystalline transition as does the 80 nm particle. For the materials parameters used here, the change in behavior to spontaneous amorphization at a critical overpotential occurs at a critical radius of $R_c = 33$nm. Although the precise numerical value for the critical size is subject to some uncertainty given the estimates used for materials variables, the significant point here is that below a

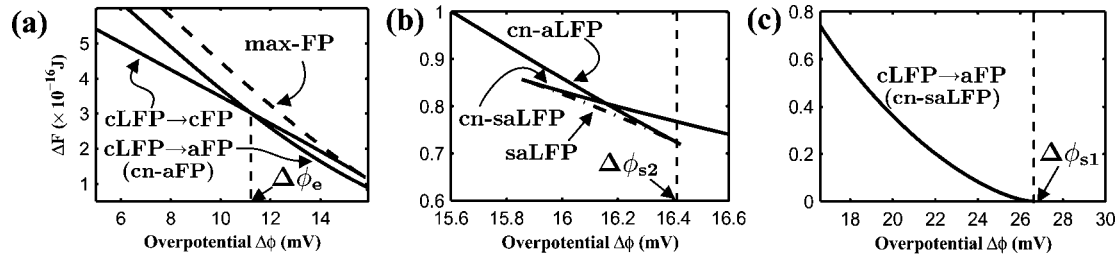

Figure 7. Overpotential dependence of the energy barrier, ΔF, for transformation of an initially crystalline $LiFePO_4$ particle to crystalline and amorphous delithiated end states by various transformation pathways, for a particle of $r_0 = 25$ nm. (a) Activation energies for the crystalline (cLFP → cFP) and amorphous (cLFP → aFP) phase transitions both decrease with increasing overpotential, and above $\Delta\phi_e = 11.21$mV, transformation to the amorphous phase becomes favored. (b) Results at a higher range of overpotentials. A cLFP particle with an SAF becomes unstable against spontaneous amorphization at $\Delta\phi_{s2} = 16.43$mV, whereas (c) one without an SAF becomes unstable to spontaneous amorphization at $\Delta\phi_{s1} = 26.56$ mV. The energies of the cn-cFP, cn-saLFP, and saLFP curves in (b) are measured relative to cLFP.

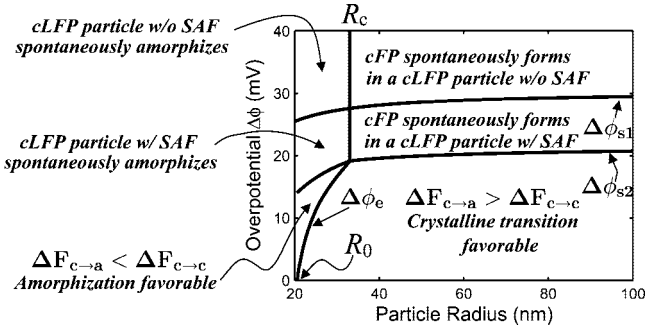

Figure 8. Phase transition map showing preferred transition pathways upon delithiation of a crystalline $LiFePO_4$ particle, as a function of the particle radius and overpotential. The phase boundaries and critical radii (R_c, R_0) are determined from the particle size dependence of the characteristic overpotentials $\Delta\phi_{s1}$, $\Delta\phi_{s2}$, and $\Delta\phi_e$ (see text). R_c is the critical radius below which spontaneous amorphization occurs, and R_0 is the critical radius for amorphization to have a smaller activation energy than the crystalline transition at all positive overpotentials. Results correspond to the case of no misfit strain between bulk phases, $\Delta e^0 = 0$.

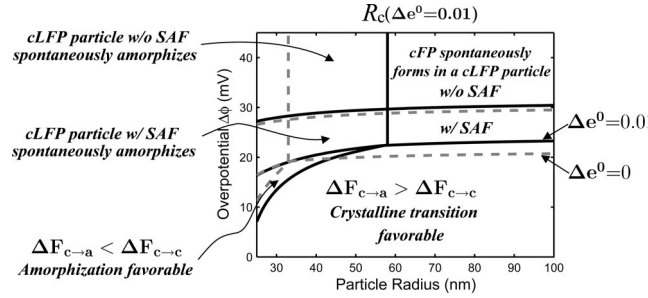

Figure 9. Phase transition map showing preferred transition pathways upon delithiation of a crystalline $LiFePO_4$ particle, as a function of the particle radius and overpotential, calculated at 1% linear misfit strain ($\Delta e^0 = 0.01$). The phase boundaries and critical radii (R_c, R_0) are determined from the particle size dependence of the characteristic overpotentials $\Delta\phi_{s1}$, $\Delta\phi_{s2}$, and $\Delta\phi_e$ (see text). R_c is the critical radius below which spontaneous amorphization occurs, and R_0 is the critical radius for amorphization to be favorable at non-negative overpotentials. The results for zero misfit strain ($\Delta e^0 = 0$) from Figure 8 are plotted in gray dashed lines for comparison.

critical size, and above a critical overpotential, spontaneous amorphization of the entire particle will occur upon delithiation. However, because the crystalline $FePO_4$ phase still has the lowest free energy among all the bulk phases at zero overpotential, the amorphous phase formed under applied overpotential is an intermediate state, and should eventually transform to crystalline $FePO_4$ phase given enough time at zero overpotential. As discussed in section V, recent experiments suggest precisely this kind of behavior.

Thus three characteristic overpotentials, $\Delta\phi_e < \Delta\phi_{s2} < \Delta\phi_{s1}$, were identified from the model. $\Delta\phi_e$ is the overpotential above which an amorphization transition has a smaller activation energy than the crystalline transition. $\Delta\phi_{s1}$ and $\Delta\phi_{s2}$ are the critical overpotentials above which a crystalline particle without or with SAF, respectively, spontaneously transforms to an amorphous particle in advance of an eventual transition to the delithiated olivine phase (if the overpotential is removed). The values of these characteristic overpotentials are size-dependent, and they do not necessarily exist at all particle sizes. By plotting the three overpotentials as a function of particle radius in Figure 8, we obtain a phase transition map that shows the preferred phase transition pathway as a function of overpotential and particle size. It shows that $\Delta\phi_e$, $\Delta\phi_{s2}$, and $\Delta\phi_{s1}$ each decrease with decreasing particle radius, and $\Delta\phi_e$ can only be found below a critical radius R_c. In particular, $\Delta\phi_e$ drops to 0 mV at a radius of $R_0 = 20.5$ nm. R_0 ($<R_c$) is therefore another characteristic radius, below which the formation of amorphous phase is favored at any positive overpotential upon delithiation.

3.4. Effect of Misfit Strain on Phase Transition Behavior. In the models presented above, the effect of lattice parameter mismatch between the lithiated and delithiated olivine phases on the phase transition energy barriers has been excluded by setting the misfit strain Δe^0 to zero. A nonzero misfit strain creates coherency stresses across the crystalline $LiFePO_4/FePO_4$ interface where a lithium concentration gradient is present, and raises the energy barrier for the crystalline delithiation transition cLFP → cFP. However, misfit strain should have little effect on the amorphous phase transition because of the incoherent nature of the amorphous/crystalline phase boundary. It is thus expected that amorphization will be increasingly favored with increasing misfit strain Δe^0. To study this effect quantitatively, we calculated the particle size−overpotential phase transition map for various misfit strain values, otherwise using the same parameters as in the last section. Starting with 1% linear strain ($\Delta e^0 = 0.01$, equal to 3% volume strain), dramatic effects are seen, Figure 9. The critical radius R_c below which spontaneous amorphization occurs increases almost 2-fold from 33 nm without strain, to 58 nm with 1% strain. Strain induces amorphization in much larger particles upon delithiation. The other characteristic radius, R_0, below which amorphization is favorable at any positive overpotential, also increases slightly, from 20.5 to 22.5 nm.

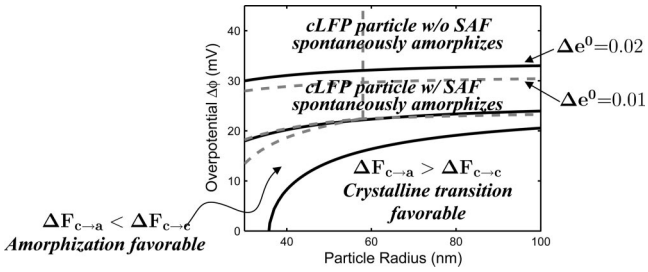

Figure 10. Phase transition map showing preferred transition pathways upon delithiation of a crystalline $LiFePO_4$ particle, as a function of the particle radius and overpotential, calculated at 2% linear misfit strain ($\Delta e^0 = 0.02$). Note that the critical radius R_c no longer appears; all particle sizes shown will undergo amorphization at large enough overpotential. The results for a misfit strain of $\Delta e^0 = 0.01$ from Figure 9 are plotted as gray dashed lines for comparison.

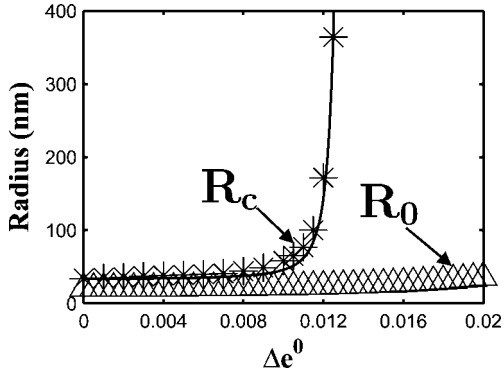

Figure 11. Misfit strain dependence of the critical radii R_c and R_0. When the particle size is smaller than R_c, amorphization occurs when the overpotential reaches a critical value. When the particle size is smaller than R_0, amorphization has a smaller activation energy than the crystalline transition even at zero overpotential. The solid line is a fit to R_c given by eq 22 of the text.

When the linear misfit strain is further increased to $\Delta e^0 = 0.02$ (6% volume strain), amorphization is found to be a competitive transition pathway at any particle size, and the critical particle size R_c is no longer found. The phase transition map for $\Delta e^0 = 0.02$ is shown in Figure 10 for particle radius up to $r_0 = 100$ nm, and does not include R_c. To further explore the critical particle sizes at which amorphization becomes the preferred pathway, we calculated the two characteristic radii, R_c and R_0, for a series of Δe^0 values between 0 and 0.02, and plot their dependence on the misfit strain in Figure 11. It shows that R_c increases almost exponentially with Δe^0 and diverges between $\Delta e^0 = 0.01$ and 0.02. R_0 also increases with Δe^0 but at a smaller rate, and remains finite at $\Delta e^0 = 0.02$. It was found that the R_c vs Δe^0 relationship can be fitted nicely by

$$R_c = 31.4 + 0.913 \exp\left(\frac{0.013}{\Delta e^0_{crit} - \Delta e^0}\right) \qquad (22)$$

where Δe^0_{crit} is a critical misfit strain above which an amorphization pathway is preferred over the crystalline delithiation transition at any particle size. For the present system, the critical strain is calculated to be $\Delta e^0_{crit} = 0.0147$, which is near the mean linear strain for the $LiFePO_4$ to $FePO_4$ transformation.[5]

The impact of misfit strain predicted by our model is especially important considering that the mean linear misfit strain between *bulk* lithiated and delithiated phases in each one of the major $LiMPO_4$ compounds of interest (M = Mn, Fe, Ni, Co) is of this magnitude (~1.5%) or larger. The implication is that unless the misfit strain is reduced through previously discussed mechanisms,[5,6] the lowest-energy transition pathway will always involve an amorphous phase. Note that this does not always require that the entire particle become amorphous. If the most stable state of the particle before and after the transition is crystalline, surface amorphization, or formation of an interfacial amorphous transition zone region between crystalline $LiMPO_4$ and MPO_4, provides a lower-energy pathway. While we only modeled the delithiation process in this work, a similar transition pathway through an amorphous phase is expected to occur upon lithiation for misfit strains of comparable magnitude, because the coherent stress across the crystalline $FePO_4/LiFePO_4$ phase boundary is essentially the same during delithiation and lithiation. Although we have assumed that the phase transitions are initiated on the surface, large particles in particular may have internal defects or interfaces at which the phase transition nucleates.[10] Clearly, mechanisms for relaxing the coherency stress across the crystalline $LiMPO_4/MPO_4$ phase boundary, such as formation of interfacial dislocations or other incoherent structures or even fracture, will be important. Modification of the lithium miscibility gap [5,6] also provides a mechanism for reducing elastic misfit, in fact below the current calculated critical value.[5] Regardless, our calculations show that misfit strain has an enormous effect on both the transformation pathway and the magnitude of the energy barrier for the transformation of crystalline olivines, and by extension other intercalation compounds.

Further refinement of the model, including the consideration of particle elastic and surface stress anisotropy and more accurate estimates of the materials parameters in Table 1, will change the phase transition maps in quantitative detail. However, the main outcomes, i.e., that amorphization becomes the preferred transition pathway below a critical particle size and at sufficiently large overpotentials, and that varying misfit strain will significantly change the size dependence of transition pathways, is expected to remain unchanged.

4. Comparison to Experiment

We first discuss chemical lithiation/delithiation experiments in which local amorphization has been observed.[10] Although the present work models the effect of electrical overpotentials, there is a direct equivalent in the thermodynamic activity of lithium imposed by a chemical oxidizer or reducer. Chen and Richardson[10] have observed that large particle samples undergoing (aggressive) chemical delithiation from bulk crystalline triphylite $LiFePO_4$ to heterosite $FePO_4$ exhibit cracking, presumably due to the large (~6.5%) volume change, but microscopically form amorphous regions at the tips of cracks. This observation is consistent with our results predicting that an amorphization pathway is preferred when the linear strain exceeds ~1.5%. The amorphous zone may be viewed as a stable transition region that relieves crystalline misfit strains which would otherwise be present. Because cracking can also relieve the misfit strain, it is likely

that the amorphous regions either formed prior to cracking when the misfit strain energy was higher, or are retained at the crack tips because residual stresses are still present in those regions. We may speculate that portions of the particle that are crystalline in this ex situ observation, such as the crack faces, may have actually recrystallized from a transient amorphous phase.

With respect to electrochemical cycling experiments, while numerous in situ and ex situ studies of the structure of olivines have been reported, to our knowledge only Meethong et al.[7] have explicitly considered amorphization as a phase transformation response. The situation is to some extent understandable because studies are typically conducted on cells containing amorphous binders, carbon additives, separators, or other components that yield large background signals. Thus newly formed amorphous phases could easily be overlooked. In comparing published experimental results to the model, we can furthermore distinguish between results obtained in the presence of an applied overpotential, for example during galvanostatic cycling or at a constant voltage hold in a PITT test, and experiments at zero overpotential, for example during the open-circuit rest in a GITT experiment. The significance of such differences has not previously been appreciated.

Meethong et al.[7] compared the zero-overpotential behavior of $LiFePO_4$ with >100 nm and <50 nm particle sizes and observed several differentiated responses. They first observed that the open-circuit voltage (OCV) of lithium half-cells exhibited very slow relaxation (>200 h) in the case of nanoscale samples, whereas for both large and small particle sizes, the OCV was dependent on the state-of-charge (SOC), in violation of strict two-phase equilibrium. (The SOC dependence of the OCV was in fact opposite in the two types of samples.) They then used X-ray diffraction (Rietveld refinement) to quantify the relative amounts of the two detectable crystalline phases, triphylite $Li_{1-x}FePO_4$ and heterosite Li_yFePO_4, as well as their specific compositions x and y, at various states of charge after open-circuit relaxation. The >100 nm size sample exhibited nearly ideal behavior in its relaxed state, with the two crystalline phases remaining nearly invariant in composition and varying linearly in amount with Li concentration (SOC). However, the nanoscale sample (34 nm) was highly nonideal—the crystalline phase compositions varied continuously with the SOC, and most importantly, the relative amounts of the crystalline phases could not be reconciled with the total Li concentration of the sample, even after relaxation. By applying the necessary mass balance conditions, Meethong et al.[7] concluded that at least one amorphous phase must coexist with the two crystalline phases. The results are consistent with the size and strain effects of the current model, e.g., Figure 10. Below a critical size (~38 nm), amorphization is the preferred transition pathway, even at zero overpotential. With increasing overpotential, amorphization is the preferred pathway even for large particles. The slow relaxation of OCV and retention of amorphous phase in the nanoscale material suggests that a greater extent of amorphization existed prior to relaxation. During the open-circuit rest there is most likely a partial recrystallization of the amorphous phase formed during the application of overpotential, but a large fraction of the sample (probably the smallest particles) remains amorphous. Meethong et al.[7] also tested $LiMnPO_4$ of 78 nm particle size, and found clear diffraction evidence for amorphization in partially charged samples. The trend is consistent with the misfit strain dependence of the transition behavior: $LiMnPO_4$ has a much larger difference in unit-cell-volume between its lithiated and delithiated phases of about 11%,[5] compared to $LiFePO_4$, in which it is 4−7% depending on the specific material. The other materials parameters for $LiMnPO_4$ are likely to be close to those used here for $LiFePO_4$, and if so, we would predict amorphization to be the preferred transition upon delithiation of $LiMnPO_4$ at any particle size, in the absence of mechanisms to relieve the strain.

Wu et al.[44] have recently reported in situ synchrotron X-ray diffraction results in which the evolution of crystalline phases in $LiFePO_4$ of 3 μm size scale (almost certainly representing an aggregate size with finer primary crystallites) was monitored during charge and discharge. During galvanostatic discharge (i.e., with applied overpotential), they observe no detectable shift in peak positions of a pre-existing $FePO_4$ phase (indicating negligible composition change in that phase, see their Figure 1), and the peaks for the lithiated $LiFePO_4$ phase barely appear. This is a clear violation of Li mass balance unless an additional, undetected phase is assumed to be present. Furthermore, they observe that upon switching to an open-circuit rest (i.e., zero overpotential) the "missing" $LiFePO_4$ phase peaks suddenly appear in the XRD pattern and grow rapidly, over the time scale of minutes. During subsequent charge, a similar behavior is seen—the $FePO_4$ phase does not grow during charging (applied overpotential), but appears rapidly once the cell is switched to rest (zero overpotential). Here also, mass balance cannot be satisfied without assuming the presence of a phase not detectable by diffraction. Wu et al.[44] refer to their results as reflecting a "frozen" state of the active material but do not comment on the lack of Li mass balance for the crystalline phases. We believe their results reflect amorphization under applied overpotential both during charge and discharge. Once the overpotential is removed, however, the stable crystalline phases rapidly form.

It should be noted that other metastable phases may also compete for stability with the amorphous phase. For example, metastable crystalline phases of unclear structure have recently been observed by Chung et al. [45] during the formation of nanocrystalline Li_xFePO_4. Also, the competition between phase transition pathways has been assessed here from the activation energies to initiate the transition (i.e., evaluating the critical nucleus state). The kinetics for propagating the phase transitions, which rely on atom diffusion rates in the respective phases, have not been considered because there are almost no data available for amorphous $LiFePO_4$. For example, if amorphization is sluggish compared to the rate of lithium transport in and

(44) Chang, H.-H.; Chang, C.-C.; Wu, H.-C.; Yang, M.-H.; Sheu, H.-S.; Wu, N.-L. *Electrochem. Commun.* **2008**, *10*, 335.
(45) Chung, S.-Y. 214th Electrochemical Society Meeting;Honolulu, HI, 2008; Electrochemical Society: Pennington, NJ, 2008; Abstract #562.

out of the crystalline phases, then the crystalline transition could dominate during high rate charging/discharging processes even if the phases present are metastable. Alternatively, the one-dimensional nature of lithium diffusion in olivine [46]compared to the isotropic diffusion expected for amorphous phases could lead to anisotropic, kinetically enhanced amorphization.

Finally, we note that the real-world use of batteries produces highly dynamic cell voltages which may cause complex time-varying phase states due to variations in overpotential. One example is the high power pulse cycling to which hybrid electric vehicle batteries are subjected. Pulse cycling may cause amorphization due to high overpotential (see Figures 8−10), followed by partial recrystallization after overpotential transients, in repeated cycles—leading to complex and hysteretic phase changes. As another example, if the kinetics of amorphization are sluggish compared to the rate of lithium diffusion in or out of the starting crystal, an overpotential may result in a metastable crystalline olivine phase that then amorphizes over time. The present work provides a framework to understand such complex phenomena.

5. Conclusions

A diffuse-interface model has been developed to assess the conditions under which the competing pathways of a crystalline-to-crystalline phase transition is preferred vs a crystalline-to-amorphous transition during the electrochemical cycling of intercalation compounds. Olivine $LiFePO_4$ has been used as the model system. The free energy includes chemical, strain, gradient, and surface energy contributions, from which the activation energies for different phase transition pathways during delithiation of an initially lithiated crystalline particle has been calculated. The effects on the transition energy barriers of (1) particle size; (2) applied electrical overpotential, and (3) misfit strain between the lithiated and delithiated phases, were evaluated numerically. For particles below a critical radius R_c, the activation energy for amorphization decreases with increasing overpotential, and becomes less than that for the crystalline transformation above a critical overpotential that is in the range 10−30 mV. Below another critical radius R_0, particles are prone to transformation via an amorphous phase even at zero overpotential. Furthermore, the behavior is extremely sensitive to the misfit strain between the lithiated and delithiated crystalline phases. The critical particle size R_c increases exponentially with misfit strain, and there is a critical value of misfit strain above which amorphization is the preferred pathway at all particle sizes, assuming no other mechanisms for relieving the strain. The results of the model are consistent with several experimental observations.

Acknowledgment. This work was supported in part by United States Advanced Battery Consortium Project DE-FC26-05NT42403. M.T. acknowledges partial support from the Lawrence Postdoctoral Fellowship. N.M. acknowledges support by the Royal Thai Government Scholarship and Y.H.K. acknowledges support by Taiwan Merit Scholarship TMS-94-2-A-019.

(46) Morgan, D.; Van der Ven, A.; Ceder, G. *Electrochem. Solid-State Lett.* **2004**, *7*, A30.
(47) Carter, W. C.; Taylor, J. E.; Cahn, J. W. *JOM−J. Miner., Met., Mater. Soc.* **1997**, *49*, 30.

Appendix

The stability of eqs 13−21 was computed with a numerical functional gradient flow in the I-2 norm[47] on the functional in eq 1. The stability of a particular state, $c(r)$ and $\eta(r)$, is iteratively minimized by introducing a (time-like) path-variable, τ. Discrete iteration, $c(r, \tau + \Delta\tau)$ and $\eta(r, \tau + \Delta\tau)$, in the direction of (minus) the functional gradient

$$\frac{\partial c(r,\tau)}{\partial \tau} = -\frac{\delta F_{\text{tot}}}{\delta c} \tag{A1}$$

$$\frac{\partial \eta(r,\tau)}{\partial \tau} = -\frac{\delta F_{\text{tot}}}{\delta \eta} \tag{A2}$$

will cause the system to evolve toward smaller F_{tot}.

At each iteration, the displacement field u is recomputed from eq 15 at all τ. The metastability of extremal solutions to eq 13−21 are evaluated by addition of a small perturbation field; then eqs A1−A2 are iterated (with numerical solution of eq 15) to determine whether the perturbation grows with τ or not. With increasing τ, eqs A1−A2 and 15 will advance $c(r,\tau)$, $\eta(r,\tau)$, and $u(r,\tau)$ along a trajectory of decreasing free energy F_{tot}, and eventually to a state corresponding to a local energy minima of F_{tot}. Therefore, if a solution to eqs 13−21 is locally stable, the initial perturbation will diminish with τ and c, η, and u will return to their original profiles. As a corollary, if $c(r, \tau = 0)$ and $\eta(r, \tau = 0)$, are maximal or saddle point fields for F_{tot}, the perturbation will grow with τ and c, η, and u will evolve to a different, locally stable state.

The saddle point character of the critical nucleus solution cn-cFP is demonstrated in Figure A1. In panels a and b in Figure A1, the concentration profile of cn-cFP is proportionally de-

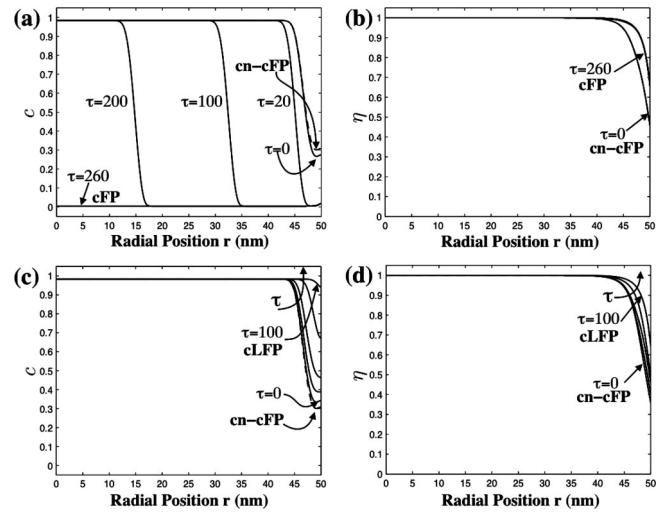

Figure A1. Evolution of lithium concentration and crystallinity of the perturbed critical nucleus state cn-cFP in a 100 nm diameter particle at $\Delta\phi = 15$ mV following eqs A1 and A2. In (a) and (b), the lithium concentration field of cn-cFP (dashed line) is initially negatively perturbed by 5%. $c(r, \tau)$ and $\eta(r, \tau)$ become indistinguishable from cFP at $\tau = 260$ in the figure. Note that the η profile of $\tau = 20$ overlaps with $\tau = 0$ on the plot, and those of $\tau = 100$ and 200 overlap with the profile of $\tau = 260$. In (c) and (d), the concentration field of cn-cFP (dashed line) is positively perturbed by 5%. The solid lines in (c) and (d represent c and η profiles at $\tau = 0$, 10, 20, 50, and 100. $c(r, \tau)$ and $\eta(r, \tau)$ become indistinguishable from cLFP at $\tau = 100$ in the figure.

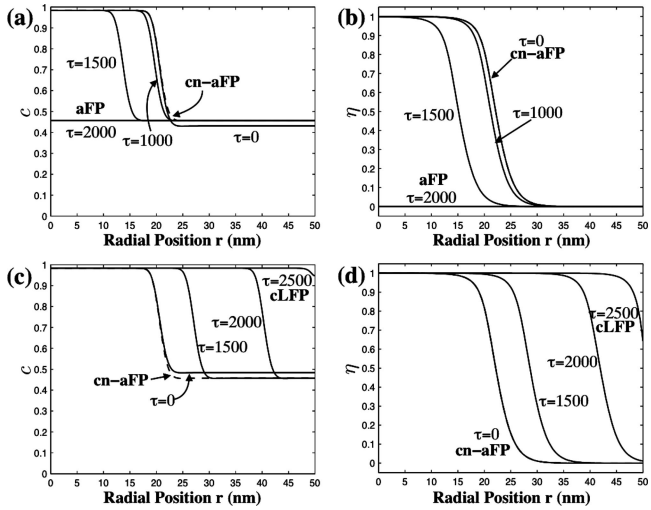

Figure A2. Evolution of lithium concentration and crystallinity of the perturbed critical nucleus state cn-aFP in a 100 nm diameter particle at $\Delta\phi = 15$ mV following eqs A1 and A2. In (a) and (b), the lithium concentration field of cn-aFP (dashed line) is initially negatively perturbed by 5%. $c(r,\tau)$ and $\eta(r,\tau)$ become indistinguishable from cFP at $\tau = 2000$ in the figure. In (c) and (d), the concentration field of cn-aFP (dashed line) is positively perturbed by 5%. $c(r, \tau)$ and $\eta(r, \tau)$ become indistinguishable from cLFP at $\tau = 2500$ in the figure.

creased (i.e, negatively decreased in Figure A1) by 5%, i.e., $c(r, \tau = 0) = c_0(r) - 0.05[c_0(r) - c_0(r = 0)]$, where $c_0(r)$ is the lithium concentration of cn-cFP. the perturbation is amplified with increasing τ and the lithium concentration and crystallinity fields eventually evolve to those of cFP. When a 5% positive proportional increase is added to the lithium concentration of cn-cFP at $\tau = 0$ instead, the particle state will evolve to cLFP at large τ, viz. panels c and d in Figure A1.

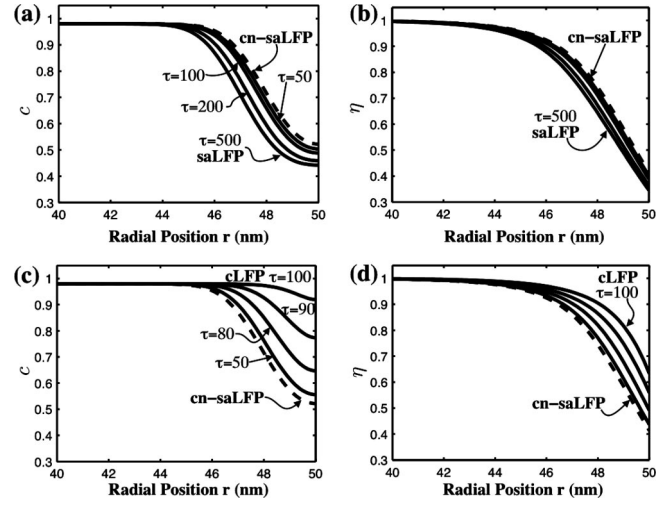

Figure A3. Evolution of lithium concentration and crystallinity of the perturbed critical nucleus state cn-saLFP in a 100 nm diameter particle at $\Delta\phi = 19.5$ mV following eqs A1 and A2. In (a) and (b), the lithium concentration field of cn-saLFP (dashed line) is initially negatively perturbed by 1%. $c(r, \tau)$ and $\eta(r, \tau)$ become indistinguishable from saLFP at $\tau = 500$ in the figure. In (c) and (d), the concentration field of cn-aFP (dashed line) is positively perturbed by 1%. $c(r, \tau)$ and $\eta(r, \tau)$ become indistinguishable from cLFP at $\tau = 100$ in the figure.

Similarly, the stability of critical nucleus states, cn-aFP and cn-saLFP, are examined by iterating eqs A1 and A2. Figures A2 and A3 illustrate that they are the saddle point states connecting two locally stable states, i.e., cLFP and aFP in the case of cn-aFP and cLFP and saLFP in the case of cn-saLFP.

CM803172S